Available online at www.sciencedirect.com
ScienceDirect
Journal of Hazardous Materials 158 (2008) 257–263
Journal of Hazardous Materials
www.elsevier.com/locate/jhazmat

Photocatalytic removal of M^{2+} (=Ni^{2+}, Cu^{2+}, Zn^{2+}, Cd^{2+}, Hg^{2+} and Ag^{+}) over new catalyst $CuCrO_2$

W. Ketir, A. Bouguelia, M. Trari *

Laboratoire de Stockage et de Valorisation des énergies Renouvelables, Faculty of Chemistry (USTHB), BP 32, 16111 Algiers, Algeria

Received 16 May 2007; received in revised form 11 November 2007; accepted 18 January 2008
Available online 16 February 2008

Abstract

The metal ions M^{2+} (Ni^{2+}, Cu^{2+}, Zn^{2+}, Cd^{2+}, Hg^{2+} and Ag^{+}) are potentially toxic. Their electro deposition has been carried out in aqueous air-equilibrated $CuCrO_2$ suspension upon visible illumination. The delafossite $CuCrO_2$ is p-type semiconductor characterized by a low band gap (1.28 eV) and a long-term chemical stability. The corrosion rate is found to be 10^{-2} μmol m^{-2} $month^{-1}$ in aqua regia. The oxide has been elaborated through nitrate route where the specific surface area is increased via the surface/bulk ratio. A correlation exists between the dark M^{2+} adsorption, the redox potential of $M^{2+/0}$ couple and the conduction band of $CuCrO_2$ positioned at $-1.06\ V_{SCE}$. Ag^{+} cannot be photoreduced because of its positive potential located far above the valence band. By contrast, Zn^{2+} is efficiently deposited due to the large driving force at the interface. The improved photoactivity of copper with a deposition percentage (90%) is attributed to the strong dark adsorption onto the surface catalyst. The results indicate a competitive effect with the water reduction; it has been observed that the M^{2+} deposition goes parallel with the hydrogen evolution. Such behavior is attributed to the low H_2 over voltage when ultra fine aggregate of M islands are photodeposited onto $CuCrO_2$ substrate.

Keywords: Photocatalytic reduction; Metal ion catalyst; Delafossite $CuCrO_2$; Nitrate route

1. Introduction

The use of renewable energies has been the subject of several researches during the last decades and continues to attract much attention owing to growing interest in the energy conversion [1,2]. We emphasize the importance of seeking new materials for the photoelectrochemical (PEC) conversion over semiconductors (SC). In fact, modern society lives in an environment with many harmful products; heavy metals (M) and their salts are toxic and pollute both air and water [3]. Most sources of harmful metals arise from industrial activities and the threshold concentration of M^{2+} poses a particular challenge for the water quality. On the other hand, the energy crisis has stimulated extensive research in the field of PEC processes whose principles have been undertaken earlier by some pioneers [4,5]. The photoelectrochemistry is based on the excitation of SC by appropriate light ($h\nu > E_g$), E_g being the forbidden band. The electric junction field that takes place spontaneously between the solid and liquid phases allows the separation of photogenerated electron/hole (e^-/h^+) pairs. The electrons in the conduction band (CB) undergo a cathodic metal reduction and/or hydrogen evolution onto the surface catalyst whereas the holes in the valence band (VB) move in the opposite direction to carry out the anodic reaction. The powder suspension is inexpensive, easy to use and the photocatalysis may be extended on large scales. The whole PEC process takes place on a single SC crystallite to avoid the bulk phase diffusion of the reactants [6]. The PEC metal deposition and the photomineralization of organic compounds is a major part of the environmental protection [7]. The ions M^{2+} are reduced to their elementary state on SC surface and can subsequently be extracted by physical and/or chemical methods.

In general, wide band gap oxides SC are found to be stable against the photodissolution but inhibit the light of the sun spectrum. UV radiation is required for their sensitization and this makes them inappropriate for the direct conversion. Two contradictory factors may govern the efficiency: the flat band potential (V_{fb}) and E_g according to the empirical relation $E_g = V_{fb} - 2.94$

* Corresponding author.
E-mail address: mtrari@caramail.com (M. Trari).

0304-3894/$ – see front matter © 2008 Elsevier B.V. All rights reserved.
doi:10.1016/j.jhazmat.2008.01.074

[8]. So far, no compound having all the characteristics, i.e. a small E_g, a positive potential V_{fb} (for p-type specimen) and a good chemical stability has been found. In this optic, our investigations have been directed towards materials with new band structure. The cuprates $CuMO_2$ which crystallize in the delafossite structure have received growing attention in the field of optoelectronic devices due to their interesting properties of band gap modulation and pH-insensitivity of the electronic bands [9]. Until recently, the recovery of metals on delafossites has never been reported. This family of oxides has attracted renewed interest because of their photocatalytic activity [10]. Given the fact that there appears to be a direct band gap SC at 1.28 eV close to the ideal value required for terrestrial applications, $CuCrO_2$ is a potential candidate for PEC conversion. The degree to which the ions M^{2+} can be deposited is determined by the band bending (B) at the interface SC/electrolyte. In presence of M^{2+}, the oxide is suitably biased to form a depletion layer leading to an efficient separation of photogenerated (e^-/h^+) pairs. We may expect that dissolved oxygen might not be reduced because of the potential of the O_2/H_2O couple ($\sim$1 V_{SCE}), located far above $CuCrO_2$-VB.

The present study combines the solar energy with the environmental protection. It deals with the reduction of the title ions M^{2+}, which takes place on $CuCrO_2$ under visible irradiation. The dark adsorption enhances the reduction process. This enabled us to determine why some metals are photoelectrodeposited whereas others are not. A correlation is established between the energy band diagram of $CuCrO_2$ and the redox potentials of M^{2+}/M couple. Limitations could have occurred due to the precipitation of hydroxides $M(OH)_2$. However, all the experiments have been conducted under mild conditions close to those found in the aquatic natural media (pH 6–7). Water competes with the M^{2+} ions for the photoelectrons and the reduction is decelerated with time. Hence, the photoactivity is also determined by measuring the volume of evolved hydrogen, but the medium pH should have facilitated the M^{2+} deposition. Interestingly, the specie showing the high H_2 evolution exhibits the stronger M^{2+} reduction. Due to the low overvoltage, the metal electrodeposition onto the crystallite mediates the H_2 evolution by lowering the barrier height of the heterosystem $M/CuCrO_2$. This leads to a situation close to ohmic contact with easy electrons transfer and an increase of the rate constants (high exchange current density). The global PEC process might be limited by the low carriers' mobility. This is ascribed to narrow electronic bands of $CuMO_2$ that derive from Cu-3d parentage [11]. For this reason, $CuCrO_2$ used in this work has been elaborated through chemical way where the amount of reaction surface per given mass ratio is increased.

2. Experimental

$CuCrO_2$ has been synthesized by chemical co-precipitation starting from CuO and $Cr(NO_3)_3{\cdot}9H_2O$. The reagents with copper to iron molar ratio (Cu/Cr = 1) have been dissolved in HNO_3 (6N). Then, the solution was evaporated in a sand bath and the resulting precipitate was denitrified over a flame until there were no NO_x fumes. The amorphous powder was finally fired 12 h at 900 °C and furnace cooled. The complete formation was confirmed by X-ray diffraction (XRD) using Cu Kα radiation ($\lambda = 0.15417$ nm). The surface area of $CuCrO_2$ was determined by the BET method using nitrogen gas as the adsorbate at liquid nitrogen temperature on ASAP 2010 micromeritics apparatus. To study the transport properties and PEC characterization, the powder was pelletized under 2.3 kbar into 13 mm diameter discs of $\sim$1 mm thickness and sintered at 1200 °C. This allowed high compactness and good mechanical properties. The density of the sample was determined to be $\sim$90% of its theoretical bulk value.

Electrical contact of less than 1 Ω resistance was established by soldering copper wires onto the back pellet with silver paint. The working electrode (WE, 1.13 cm^2) was encapsulated in a glass tube and isolated by epoxy resin. A conventional three-electrode cell was used for PEC measurements, it includes a Pt sheet electrode (1 cm^2) and a saturated calomel electrode to which all the potentials were scaled. WE was illuminated by a 200-W tungsten lamp (Osram) through a flat window and the potentials were monitored by a Voltalab 40 potentiostat (the same that was used for the capacity measurements). The electrolyte (KOH 1 M) was continually flushed with nitrogen and the experiments were performed at room temperature. Photocurrent–photovoltage ($U_{ph} - J_{ph}$) plots were recorded in a two-electrode cell with external resistance boxes and two multimeters. The power density of the incident light was determined to be 30 m W cm^{-2}. The point of zero zeta potential (pzzp) has been accurately determined by measuring the equilibrium pH of an aqueous solution containing a suspension of powdered oxide.

The photocatalysis was carried out in an experimental setup previously described in detail [12]. In brief, the photocatalytic tests were performed in a double wall cylindrical Pyrex cell containing 500 cm^3 of the solution (30 ppm M^{2+}) to which 0.25 g of catalyst was added. The pH was adjusted to $\sim$6–7 and the air equilibrated solution was magnetically stirred. Two tungsten lamps ($\times$200 W) disposed diametrically around the reactor were used as light sources. The aliquots (5 cm^3) were taken at periodic time to determine the concentration of M^{2+}. After decantation, the analysis was carried out by inductively coupled plasma (ICP, Varian Vista-Pro-CCD, and Simultaneous ICP-OES). The concentration was evaluated by interpolation from a calibration curve. To determine the quantum efficiency (η), the light intensity was measured by a digital flux meter (Testo 545) without correction for solution absorbance. The procedure and the apparatus for H_2 evolution have been described elsewhere [13]. The volume was measured by water displacement from an inverted graduated burette. Blank experiments have been performed in the dark without catalyst. All the solutions have been prepared with deionized water and analytical reagents grade.

3. Results and discussion

The photoactivity is strongly dependent on the preparative conditions**.** The light conversion yield increases with the specific surface area and M^{2+} is deposited efficiently over a large area collector/convertor. $CuCrO_2$ was synthesized via nitrate route in order to increase the porosity and hence the active surface

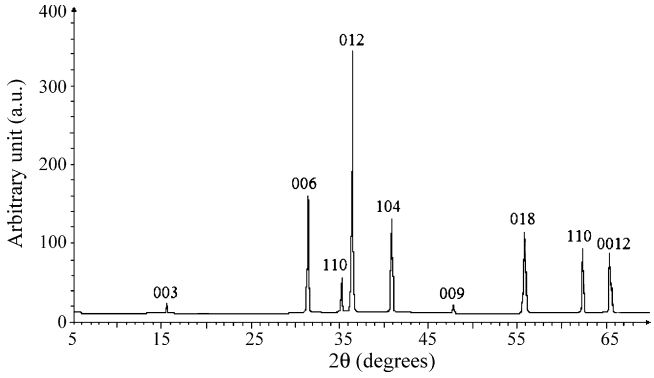

Fig. 1. XRD pattern of $CuCrO_2$, elaborated by nitrate route. All peaks are indexed on the basis of rhombohedral unit cell (SG : $R\bar{3}m$).

[14]. The end product, characterized by XRD (Fig. 1), reveals a homogeneous single phase with a dark brown color. No extra peaks due to secondary impurities such as spinel $CuCr_2O_4$, were found in the pattern. The lattice constants $a = 297.5(6)$ and $c = 171.0(2)$ pm are in perfect agreement with those given in the literature [15]. The crystallite size L (32 nm) was estimated from the full width at half maximum (FWHM) (β) of the most intense peak (0 1 2) through the relation $\{L = 0.94\lambda/\beta \cos\theta\}$, θ being the diffraction angle [16]. Assuming the crystallites to be spherical and non-porous, the specific surface area ($18 \pm 4\ m^2\ g^{-1}$) was deduced from the relation $\{=6/(Ld_{exp})\}$, d_{exp} ($5.50\ g\ cm^{-3}$) being the experimental density. The specific surface area, determined by the BET method, was found to be larger ($24\ m^2\ g^{-1}$) than that estimated from FWHM. The closeness of the two values shows that $CuCrO_2$ prepared by the nitrate route exhibits a low porosity. This shows that FWHM can give a useful but rough approximation of the active surface for weakly porous oxides.

The gradual increase in the optical absorption with decreasing wavelength, observed in the diffuse reflectance spectrum is a characteristic of direct transitions (Fig. 2). The plot of $(\alpha h\nu)^{2/n}$ versus the incident light ($h\nu$) allows the determination of both E_g and the nature of the optical transition. n is equal to 1 or 4, respectively for direct and indirect transitions. The extrapolation of $(\alpha h\nu)^2$ to the $h\nu$ axis (Fig. 2, inset) yields a direct gap of 1.28 eV very close to that reported by others [17].

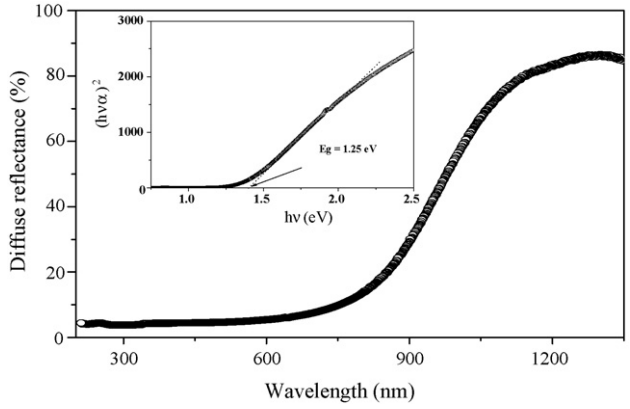

Fig. 2. Diffuse reflectance spectrum of $CuCrO_2$. Inset: direct optical transition.

$CuCrO_2$ exhibits an excellent chemical stability over the whole pH range. However, taking into consideration practical uses, chemical stability tests have been continuously performed for 6 months. The corrosion rates in the perchloric acid and aqua regia, determined from the titration of dissolved copper, were found to be 2.9×10^{-4} and $10^{-2}\ \mu mol\ m^{-2}\ month^{-1}$, respectively. By contrast, upon visible light and in the absence of suitable electroactive specie in solution, the holes may react with the lattice ions ($Cu^{+}_{lattice} + h^{+} \rightarrow Cu^{2+}_{solution}$) as evidenced by the apparition of the blue complex $Cu(H_2O)_6{}^{2+}$ whose coloration deepens with illumination time. The photodissolution is connected with H_2 evolution and it corresponds to the rate of electron accumulation (see below). A value of $\sim 6\ \mu mol\ m^{-2}\ h^{-1}$ was obtained in a solution that contains 30 ppm of Zn^{2+}.

The transport properties of $CuMO_2$ are dependent on their compositions, particularly on the deviation from stoichiometry. Oxygen inserts reversibly in the layered lattice and to achieve the electro neutrality, the nominal oxidation state of copper increases and the conductivity σ is enhanced. This should allow the oxide to be used as photoelectrode and characterized photoelectrochemically, considering its interest for the photocatalysis. $CuCrO_2$ exhibits p-type behavior and the thermal evolution of σ follows an Arrhenius-type law with an activation energy ΔE_σ of 0.22 eV that is close to that given in Ref. [9].

The intensity–potential J (V) curve in KCl media was initiated from 1 V and scanned towards the anodic direction. The dark current J_d is less than $2\ mA\ cm^{-2}$, indicating a good electrochemical stability. The sum of H_2 and O_2 over voltages does exceed 0.8 V. The significant J_d above $\sim$0.82 V is due to H_2O oxidation (O_2-bubbles are noticeable on the electrode). The anodic peak at $\sim$0.40 V (Fig. 3, inset a) corresponds to the electrochemical couple $Cu^{2+/+}$ in agreement with the value reported in Ref. [18]; the charge neutrality induces the oxidation

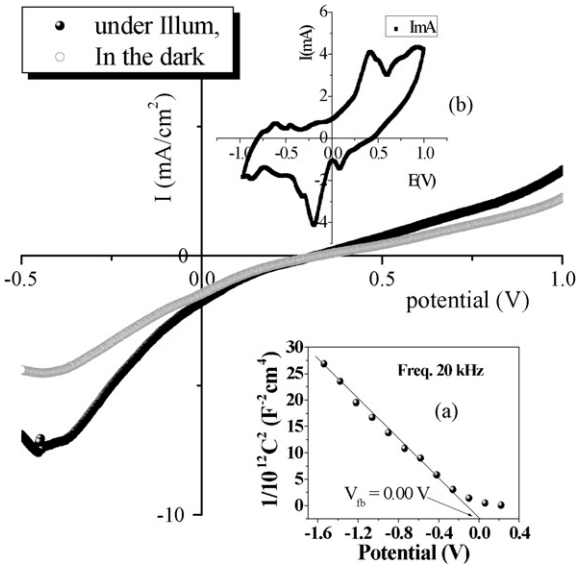

Fig. 3. The J (V) characteristics of p-type $CuCrO_2$ plotted both in the dark and under illumination in KCl (1 M). Inset a: cyclic J (V) curve in the dark showing the insertion and desinsertion of oxygen. Inset b: the Mott Schottky plot in KCl (1 M).

of $CuCrO_2$ and the reaction can be formulated:

$$CuCrO_2 + 2\delta OH^- \rightarrow CuCrO_{2+\delta} + \delta H_2O + 2\delta e^-$$

δ stands for the quantity of intercalated oxygen in the layered lattice. Another peak, appearing at ~0.7 V, is ascribed to the electrochemical couple $Cu^{3+/2+}$ and which is close to that existing in La_2CuO_4 highlighted by Grenier et al. [19]. The oxygen insertion is reversible, the peaks located at ~0.05 and −0.2 V, upon back scanning, correspond respectively to $Cu^{3+/2+}$ reduction and $Cu^{2+/+}$.

The shape of the J_{ph} (V) curve and the increase of the photocurrent J_{ph} in the negative-going potential confirms the p-type conductivity, i.e. the majority carriers are holes. J_{ph} starts to flow at +0 V and rises slowly before reaching saturation, a behavior ascribed to a negligible recombination rate of (e^-/h^+) pairs. At sufficient negative potentials, J_{ph} reaches a limiting value that has a magnitude which depends only on the light intensity. The potential (V_{on}) at which J_{ph} appears is assimilated to V_{fb}. However, V_{fb} was accurately determined from the differential capacitance:

$$C^{-2} = \{0.5e\varepsilon\varepsilon_0 N_a\}\left\{\Delta U - \frac{kT}{e}\right\}$$

in this relation, all the symbols have their usual meanings. (Fig. 3, inset b) gives the potential V_{fb} (0.04 V) from the intercept of the V-axis at $C^{-2} = 0$. The small difference with V_{on} indicates a quasi absence of surface sites within the gap region. A strong agitation does not improve significantly the photoactivity and implies that the mass transport in the electrolyte is not the rate-determining step. Indeed, the slow decrease of J_d on illumination shutdown is indicative of the slow transfer of electrons which takes place through an injection mechanism. Hence, the net PEC process is governed exclusively by the electron flow within the diffusion length. The photocatalytic properties of $CuMO_2$ arise from CuO_3^{2-} entities. The crystal structure consists of close packed sheets of octahedral sites Cr^{3+} ions sharing common edges [20]. Two adjacent layers are linked to each other by bridged monovalent copper to $\{O–Cu–O\}^{2-}$ units parallel to the [0 0 1] direction. Both electronic bands are made up mainly of Cu-3d wave function; the lower filled t_{2g} orbital that provides VB, though being non-bonding, is separated by ~2 eV from the lower lying O:2p whereas CB consists of empty hybridized dz_2/4s. This yields a high energetic position of CB and consequently a strong reducing ability of photoelectrons.

3.1. Photocatalysis

The above characterizations lead to the establishment of the energy band diagram $CuCrO_2/M^{2+}$ (Fig. 4) which predicts thermodynamically if the M^{2+} deposition and/or hydrogen liberation occur upon visible light or not. $CuCrO_2$-CB (−1.06 V), calculated from the relation ($V_{fb} + \Delta E - E_g$), is located below the redox potential E_{red} of the most $M^{2+/0}$ couples and should theoretically give a spontaneous reduction. In addition, the diagram clearly shows that the driving force decreases when the potential $E_{red.}$ of $M^{2+/0}$ couple increases and this should attenuate the reduction process.

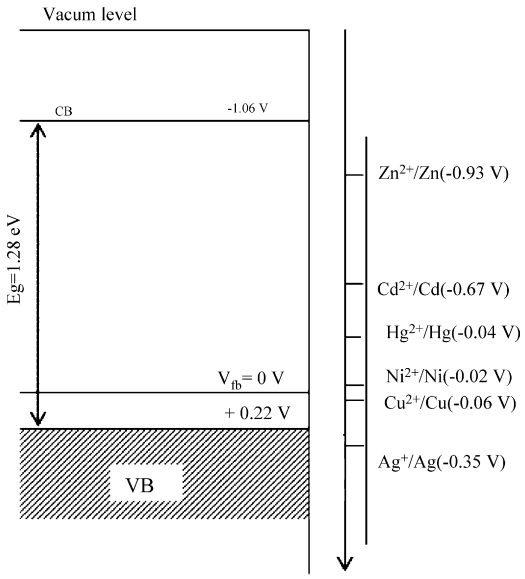

Fig. 4. Position of the valence and conduction bands of $CuCrO_2$ together with the redox potentials of involved M^{2+} (30 ppm) at pH ~ 6.

Porous oxides with large surface area are desirable in photocatalysis. Although not a general rule, the photoactivity is intrinsically determined by the properties of the material through the active surface. For $CuMO_2$, the PEC performance increases when the crystallite size decreases [10]. $CuCrO_2$ exhibits a dark adsorption for the ions M^{2+}, so a transition period is required before irradiation. The adsorption is strongly pH sensitive but the influence has not been investigated. The equilibrium time is a function of the nature of M^{2+}; it follows a cationic type adsorption and is less accentuated at low pH. The pzzp, the pH at which the net adsorbed surface is zero, was found to be 7.6 for $CuCrO_2$ and the experiments have been done in natural media around this pH. The potentials ($E_{red.}$) measured under working conditions and the dark adsorption time, i.e. the tendency of M^{2+} to be adsorbed onto $CuCrO_2$, were determined from the chrono potentiometric curves (Fig. 5). Table 1 summarizes the main results and copper exhibits by far the largest adsorption. The initial M^{2+} concentration was 30 ppm and the adsorption generally occurs within 1–2 h. However, the powder was kept in the dark overnight to ensure that M^{2+} has been adsorbed. The difference between the nominal concentration and the concentration measured after the equilibrium time was taken as the quantity of adsorbed M^{2+} onto the catalyst surface. For example, 5% of Hg^{2+} were adsorbed whereas silver exhibited a very weak adsorption affinity with only 1% of the initial concentration.

The efficiency of the charges separation depends on the existence of a space charge region. In order to collect most photoelectrons, a cathodic voltage must be applied to the oxide, which generates a depletion width (W) at the interface as is well known in the electrochemistry of semiconductors [21]. The difference ($|V_{fb} - E_{red.}|$) measures the driving force of the junction and for a zero (e^-/h^+) pairs recombination, a value of at least 0.3 V is needed [22]. The presence of M^{2+}, suitably positioned with respect to $CuCrO_2$-CB, yields a large band bending (Table 1) and the resulting electric field permits an efficient sep-

Table 1
The main characteristics of M^{2+} deposition and H_2 evolution over $CuCrO_2$

Metal	$[M]_{ads}$ (ppm)	Time (min.)	% [M] deposed in the dark	% deposition by photocatalysis	Time (min.)	η% $[M]_{dep.}$	Volume of H_2 at saturation (cm^3)	η% H_2
Cu	9	34	70	90	10	0.020	0.80	0.039
Ni	∼30	210	∼0	6	10	0.040	0.70	0.011
Zn	26	40	12	53	5	0.070	1.05	0.039
Cd	23	80	23	73	5	0.050	0.25	0.017
Hg	28	120	5	87	6	0.033	0.25	0.039
Ag	∼30	16	∼0	20	120	0.044	0.30	0.033

aration of (e^-/h^+) pairs. At constant bias, the width W given by $\{2\,\varepsilon\varepsilon_0\Delta U/eN_a\}^{0.5}$ is fixed. So, an additional condition to eventuate photoreductions is that the free potential (U_f) of p-$CuCrO_2$ must be negative of the potential V_{fb}. The best case is when the potential U_f belongs to the plateau region in the J_{ph} (V) plot. This seems to occur in our case and indicates that one can reach the limiting photocurrent without biasing the electrode to a large extent. The crystallite is by itself polarized at a potential equal to U_f (−0.93 V) and works independently like a micro-PEC cell. With a fill factor of 0.28 estimated from the power characteristics ($U_{ph} - J_{ph}$) in KCl electrolyte, $CuCrO_2$ appears to be a promising SC for PEC conversion.

The electronic bands of $CuCrO_2$, deriving from Cu-3d orbital, are fixed whatever the pH of the solution and a correlation exists between the potential $E_{red.}$ of M^{2+}/M couple and CB-$CuCrO_2$. According to the energy band scheme (Fig. 4), we can expect that Zn^{2+} and Cd^{2+} might be reduced preferentially. The ions M^{2+} which have a negative potential and good adsorption affinity, have been reduced efficiently on $CuCrO_2$ (Fig. 6). In contrast, no measurable photoreduction was observed with Ag^+ due to its low affinity for $CuCrO_2$ and its potential located above VB. The

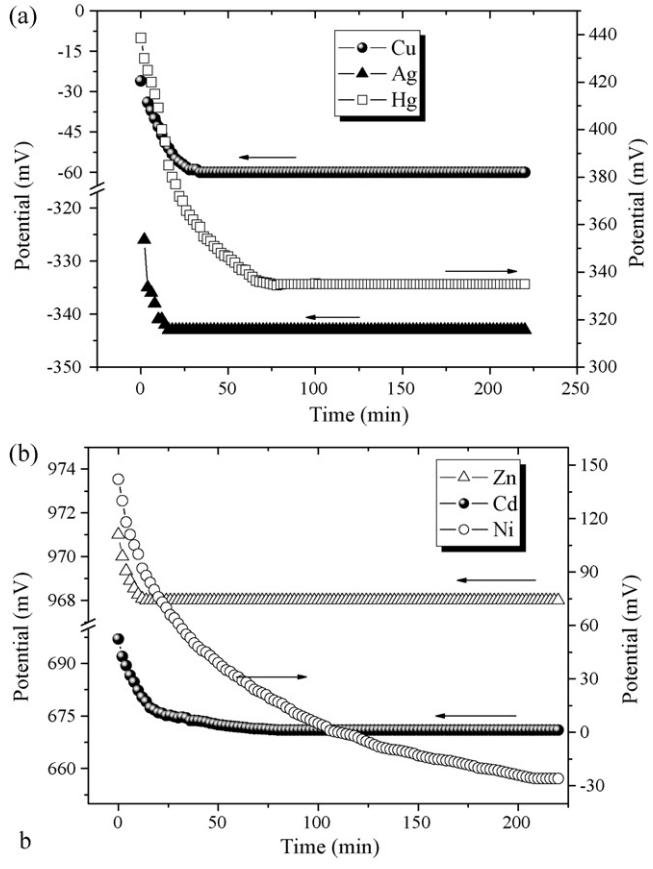

Fig. 5. (a) Chrono potentiometric curves of M^{2+} ions (M = Cu, Ag, Hg) over the powder catalyst. Adsorption of 30 ppm of M^{2+} onto $CuCrO_2$ (500 mg L^{-1}). (b) Chrono potentiometric curves of M^{2+} ions (M = Zn, Cd, Ni) over the powder catalyst. Adsorption of 30 ppm of M^{2+} onto $CuCrO_2$ (500 mg L^{-1}).

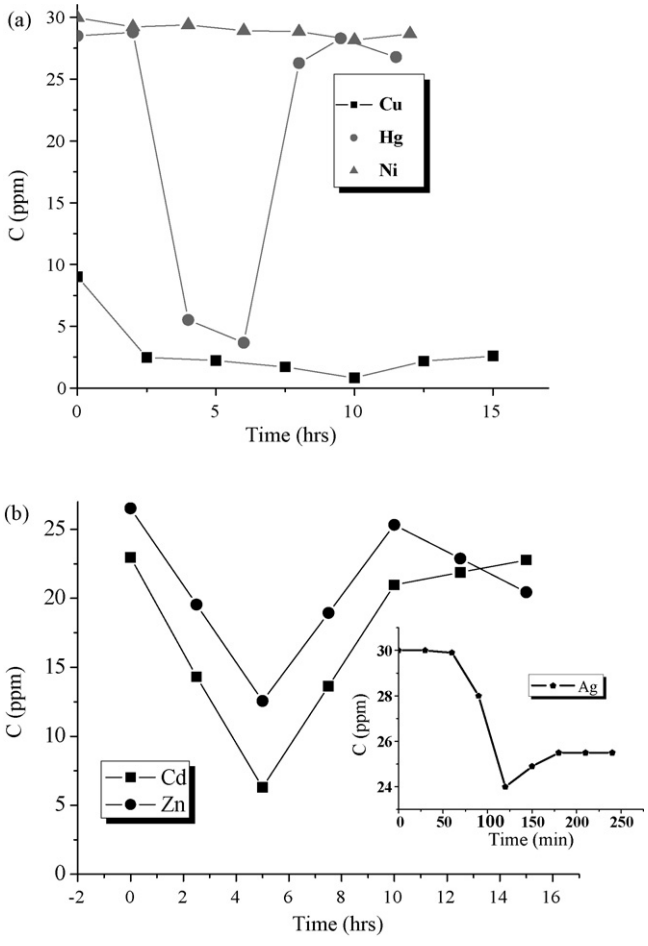

Fig. 6. (a) Photocatalytic reduction of M^{2+} (M = Cu, Hg, Ni) in air saturated $CuCrO_2$ suspension. Inset: Ag^+ titration by potentiometry (see text). (b) catalytic reduction of M^{2+} (M = Cd, Zn) in air saturated $CuCrO_2$ suspension. Inset: Ag^+ titration by potentiometry (see text).

M^{2+} reduction occurs via CB process:

$$CuCrO_2 + h\nu \xrightarrow{h\nu \geq E_g} CuCrO_2\,(h^+_{VB} + e^-_{CB}) \quad (1)$$

$$M^{2+} + 2e^-{}_{CB} \rightarrow M_{\downarrow} \quad (2)$$

$$2H_2O + 2e^- \rightarrow H_2 + 2OH^- \quad (3)$$

The metals were deposited in the first hours, but in some cases (Hg^{2+}, Zn^{2+} and Cd^{2+}) further irradiation regenerates M^{2+}. This is due to the fact that the coordinate (pH, potential) falls in the region of corrosion in the Pourbaix diagram [23] and this produces a re-oxidation of adsorbed metal. Another eventuality is the oxidation/desorption or a re-oxidation of M by holes via VB process. In any case, the rates of oxidation/reduction balance each other leading to exchange equilibrium and a tendency towards saturation. Ag^+ shows no or very low reduction. It is known that when exposed to visible light, Ag^+ undergoes a photochemical reduction but the color of the solution did not vary in our case, a result confirmed by the potentiometric titration with KI (AgI is the more insoluble salt among halides) (inset, Fig. 6b). For copper, the relatively good photoreduction is attributed to its dark adsorption. The increase of Cu^{2+} concentration after ~10 h illumination is ascribed to the photodissolution of $CuCrO_2$ and not to the corrosion of copper. This is due to the fact that the point (pH, potential) belongs to the immunity region in the Pourbaix diagram since the solution does not contain any reducing agent. Indeed, the M^{2+} reduction takes place concomitantly with oxidation by photoholes in heterogeneous photocatalysis. The blue coloration is attributed to the hexa aqua complex $Cu(HO)_6{}^{2+}$. The quantity of released copper is connected to the volume of liberated hydrogen (0.7 cm^3) on the assumption that each hole produces one Cu^{2+}. The increase of the Cu^{2+} concentration after ~10 h (1.7 ppm), easily visible on the curve (Fig. 6a), corresponds to a volume of H_2 (0.65 cm^3), a value in good agreement with that obtained in the solution containing 30 ppm of Cu^{2+} corresponding to 0.7 cm^3 of hydrogen. It is helpful to outline that the addition of a reducing agent increases the quantum yield. The holes located in VB should be efficiently scavenged, thereby lowering the rate of the recombination process of (e^-/h^+) pairs. As outlined in Table 1, we can conclude that the quantum efficiency (η) of metal photodeposition is attributed to the strong dark adsorption of M^{2+} on the surface which facilitates the photoreduction process. Then only the metals that have an absorption affinity and a potential less negative than $CuCrO_2$-CB can be photodeposited.

We observed that the M^{2+} reduction proceeds competitively with the H_2 evolution and this leads to leads to a decrease in M-deposition over time. The photoelectrons can reduce either water or M^{2+} ions depending on the pH of the solution. This is important for the solar energy conversion when a particular product is desired. The $M^{2+/0}$ couples and the $CuCrO_2$ electronic bands are pH-insensitive. The potential hazards of hydrogen does not present a handicap because it is produced in small amounts particularly at pH ~ 7 [10], is weakly soluble in water and can be easily recovered. Theoretically, a pH variation does not change significantly the degree of reduction. By contrast, the potential of H_2O/H_2 usually varies with a change of pH −0.059 V pH^{-1}. Hence, it is advantageous to shift the H_2O/H_2 level adequately with respect to CB by varying the pH. The potential of H_2O/H_2 can be located anywhere and the value at which the corresponding curve cuts the potential axis is a function of the oxygen partial pressure. A value of ~−1.2 V is obtained in an aqueous air-equilibrated solution. The experiments were conducted under mild conditions near to that observed in the aquatic media (~25 °C and pH ~6–7) and this make the M^{2+} reduction thermodynamically favorable over the H_2 evolution. Curiously, Table 1 shows that the greater the volume of evolved H_2 is, the more efficient the photoelectrodeposition of M^{2+}. So, the question that needs to be asked now is why is the water reduced easily after the powder suspension was ~6 h old (depending on M)? It is well known that the metals appear to be suitable candidates for the water discharge as they are distinguished by small over voltages. Once the metal M is photoelectrodeposited onto $CuCrO_2$, the H_2 evolution proceeds in a non-homogeneous fashion. It can affect both the type of reaction and the interfacial charge transfer rate and hence the global efficiency. Inter grains potential barrier is lowered, and the electrons are channeled towards M catalytic sites where over voltages are generally low (except for mercury). This prediction has found an experimental confirmation, and the curves of H_2 evolution are illustrated in Fig. 7. The quantum efficiency (η) is defined as

$$\eta\%[M]_{dep.} = \frac{2(\text{number of atoms M deposited})}{(\text{input number of photons})}$$

$$\eta\%H_2 = \frac{2(\text{number of molecules of } H_2)}{(\text{input number of photons})}$$

The factor 2 enters in the relation because both the H_2 evolution and the M-deposition (except for silver) are two electrons events. The η values, listed in Table 1, are apparent since the light is absorbed and reflected by the solution and the catalyst particles. In a closed system, the H_2 photoevolution stops after ~2 h. This is attributed to the fact that the potential of H_2O/H_2

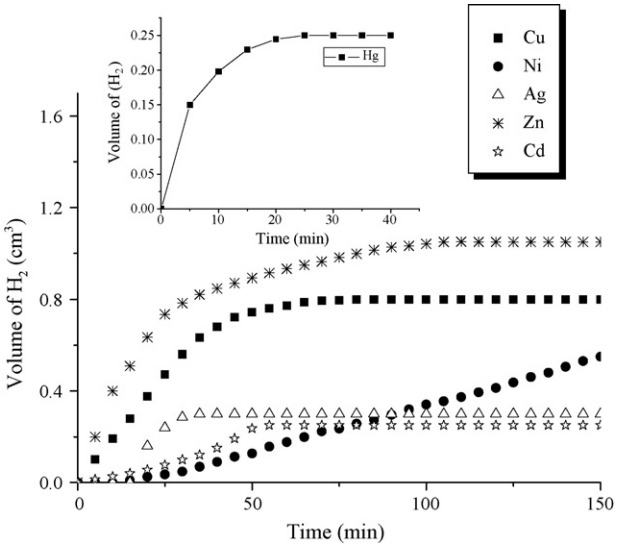

Fig. 7. Volume of evolved H_2 vs. irradiation time in solutions containing 30 ppm of M^{2+}.

couple moves towards the negative direction and lowers the band bending at the interface. The result is an increase of the rate of the recombination process of (e^-/h^+) pairs.

With a solar constant of 2300 kW/m^2 and an annual sunshine duration averaging 3000 h, the sun represents practically a clean and inexhaustible energy supply. In addition, the catalyst exhibited no sign of degradation after several cycles. This was evident from the fact that once the powder was regenerated by etching in nitric acid to remove most adsorbed metals; the initial performance was restored. These characteristics make the photocatalysis advantageous with respect to currently used techniques for the metal removal.

4. Conclusion

This study focuses on the reduction of some environmentally harmful metal ions M^{2+} which takes place on the delafossite $CuCrO_2$ upon visible light. We successfully synthesized $CuCrO_2$ by chemical way in order to increase the surface/bulk ratio. The oxygen insertion yields p conductivity which allowed PEC characterization and the establishment of the energy band diagram. The oxide is inexpensive, possesses a small forbidden band and exhibits a long-term chemical stability. These features make it attractive for the photoelectrodeposition of M^{2+} ions. The conduction band is more negative than the potential of most ions M^{2+} leading to a thermodynamically feasible photoreduction. The experiments have been performed in air-equilibrated suspension to be as close as possible to the natural environment. The photoactivity of $CuCrO_2$ is directly related to the increase of the specific surface area which accentuates the dark adsorption. M^{2+} could have been reduced to M^0 but the photoreduction no longer held if the M^{2+} adsorption is weak. The time deposition is less than 10 h during which the oxidation of some metals occurs through the corrosion process according to the potential–pH diagram. The M^{2+} deposition takes place in competition with the water reduction and exhibits a tendency towards saturation. Interestingly, the specie giving the high H_2 evolution shows the higher M^{2+} reduction. The medium pH should have made the M^{2+} deposition easier but with time it became disfavored over the water reduction. The reason is that the hydrogen evolves over the M-islands with lower overvoltages.

Acknowledgements

The authors wish to express their thanks to Mr. S. Omeiri for his technical assistance and stimulating discussions. Thanks are also to Mr. B. Biri for his constant encouragement throughout the course of this work. The work was supported financially by the Faculty of Chemistry (Algiers).

References

[1] I. Dincer, Renewable energy and sustainable development: a crucial review, Renew. Sust. Energy Rev. 4 (2000) 157–175.
[2] A. Hepbasli, Z. Utlu, Evaluating the energy utilization efficiency of Turkey's renewable energy sources during 2001, Renew. Sust. Energy Rev. 8 (2004) 237–255.
[3] D. Chen, A.K. Ray, Removal of toxic metal ions from wastewater by semiconductor photocatalysis, Chem. Eng. Sci. 56 (2001) 1561–1570.
[4] H. Gerisher, Heterogeneous electrochemical systems for solar energy conversion, Pure Appl. Phys. 52 (1980) 2649–2667.
[5] A.J. Bard, L.R. Faulkner, Electrochemical Methods: Fundamentals and Applications, 2nd ed., Wiley, New York, 2001.
[6] N. Koriche, A. Bouguelia, M. Trari, Photo catalytic hydrogen production over new oxide $CuLaO_{2.62}$, Int. J. Hydrogen Energy 31 (2006) 1196–1203.
[7] S.E. Manahan, Environmental Chemistry, 8th ed., CRS Press, New York, 2005.
[8] D.E. Scaife, Oxide semiconductors in photo electrochemical conversion, Sol. Energy 25 (1980) 41–54.
[9] F.A. Benko, F.P. Koffyberg, Preparation and opto-electronic of semiconducting $CuCrO_2$, Mater. Res. Bull. 21 (1986) 753–757.
[10] M. Younsi, A. Aider, A. Bouguelia, M. Trari, Visible light induced hydrogen over $CuFeO_2$ via $S_2O_3^{2-}$ oxidation, Sol. Energy 78 (2005) 574–580.
[11] P. Dordor, A. Chaminade, A. Wichainchai, E. Marquestaut, G.P. Doumerc, M. Pouchard, Crystal growth and electrical properties of $CuFeO_2$ single crystal, J. Solid State Chem. 75 (1988) 105–112.
[12] R. Brahimi, Y. Bessekhouad, A. Bouguelia, M. Trari, $CuAlO_2/TiO_2$ heterojunction applied to visible light H_2 production, J. Photochem. Photobiol. A 186 (2007) 242–247.
[13] S. Saadi, A. Bouguelia, M. Trari, Photo catalytic hydrogen evolution over $CuCrO_2$, Sol. Energy 80 (2006) 272–280.
[14] S. Saadi, A. Bouguelia, M. Trari, Photoassisted hydrogen evolution over spinel CuM_2O_4, Renew. Energy 31 (2006) 2245–2256.
[15] J.P. Doumerc, A. Ammar, A. Wichainchai, M. Pouchard, P. Hagenmuller, On magnetic properties of some oxides with delafossite-type structure, J. Phys. Chem. Solids 48 (1986) 37–43.
[16] B.D. Cullity, Elements of X-ray Diffraction, 2nd ed., Addison-Wesley, London, 1978, p. 102.
[17] A. Ammar, A. Wichainchai, J.P. Doumerc, M. Pouchard, Comparison between the photocurrent spectra of $CuAlO_2$ and $CuCrO_2$ electrodes, C.R. Acad. Sci. 5 (1986) 303–305.
[18] D.R. Lide, Handbook of Chemistry and Physics, 78th ed., CRC press, Florida, 1997–1998.
[19] J.C. Grenier, A. Wattiaux, N. Lagueyte, J.C. Park, E. Marquestaut, J. Etourneau, M. Pouchard, A new superconductor obtained by electrochemical oxidation of La_2CuO_4, Physica C 173 (1991) 139–144.
[20] R.D. Shannon, D.B. Rogers, C.T. Prewitt, Chemistry of noble oxides, synthesis and properties of ABO_2 delafossite compounds, Inorg. Chem. 10 (1971) 713–718.
[21] V.A. Myamlin, Y.V. Pleskov, Electrochemistry of Semiconductors, Plenum, New York, 1967.
[22] H. Gerisher, in: B.O. Seraphin (Ed.), Photoelectrolysis under Solar Irradiation at Use of Semiconductor Electrodes. Solar Energy Conversion. Solid-State Physics Aspects, Springer-Verlag, Berlin, 1982, pp. 106–150.
[23] M. Pourbaix, Atlas d'Equilibres Electrochimiques, Gauthiers-Villards, Paris, 1963.